Journal of Environmental Management 166 (2016) 579–588

Contents lists available at ScienceDirect

Journal of Environmental Management

journal homepage: www.elsevier.com/locate/jenvman

Research article

Simultaneous removal of Ni(II), As(III), and Sb(III) from spiked mine effluent with metakaolin and blast-furnace-slag geopolymers

Tero Luukkonen [a, b, *], Hanna Runtti [b], Mikko Niskanen [b], Emma-Tuulia Tolonen [b], Minna Sarkkinen [a], Kimmo Kemppainen [a], Jaakko Rämö [c], Ulla Lassi [a, d]

[a] Kajaani University of Applied Sciences, Kuntokatu 5, FI-87100, Kajaani, Finland
[b] University of Oulu, Research Unit of Sustainable Chemistry, FI-90014, University of Oulu, Finland
[c] University of Oulu, Thule Institute, FI-90014, University of Oulu, Finland
[d] University of Jyvaskyla, Kokkola University Consortium Chydenius, Unit of Applied Chemistry, Talonpojankatu 2B, FI-67100 Kokkola, Finland

ARTICLE INFO

Article history:
Received 25 June 2015
Received in revised form
26 October 2015
Accepted 6 November 2015
Available online 18 November 2015

Keywords:
Geopolymer
Metakaolin
Blast-furnace slag
Adsorption
Mine-water treatment

ABSTRACT

The mining industry is a major contributor of various toxic metals and metalloids to the aquatic environment. Efficient and economical water treatment methods are therefore of paramount importance. The application of natural or low-cost sorbents has attracted a great deal of interest due to the simplicity of its process and its potential effectiveness. Geopolymers represent an emerging group of sorbents. In this study, blast-furnace-slag and metakaolin geopolymers and their raw materials were tested for simultaneous removal of Ni(II), As(III) and Sb(III) from spiked mine effluent. Blast-furnace-slag geopolymer proved to be the most efficient of the studied materials: the experimental maximum sorption capacities for Ni, As and, Sb were 3.74 mg/g, 0.52 mg/g, and 0.34 mg/g, respectively. Although the capacities were relatively low due to the difficult water matrix, 90–100% removal of Ni, As, and Sb was achieved when the dose of sorbent was increased appropriately. Removal kinetics fitted well with the pseudo-second-order model. Our results indicate that geopolymer technology could offer a simple and effective way to turn blast-furnace slag to an effective sorbent with a specific utilization prospect in the mining industry.

1. Introduction

The presence of toxic metals and metalloids such as Ni, As, and Sb in water resources is a global concern. Aqueous Ni, As, and Sb cause acute poisoning at elevated concentrations, and prolonged exposure to lower levels can be carcinogenic (IARC, 1989; IARC, 1990; IARC, 2012). One anthropogenic contributor of Ni, As, and Sb to the aquatic environment is mining operations. However, natural dissolution of geological formations also causes groundwater contamination. Elevated arsenic levels (up to several mg/L) in groundwater are frequently found in Argentina, Chile, China, Taiwan, and Mexico, among other countries (IARC, 2004). As and Sb are chemically similar and often occur together (An and Kim, 2009; Lehr et al., 2007). An example of a mining-affected area is Prestea in Ghana, where groundwater concentrations for As and Sb can be up to 0.9–8.25 mg/L and 0.09–0.75 mg/L, respectively (Serfor-Armah et al., 2006). On the other hand, in groundwater with pH < 6.2, Ni concentrations of up to 0.98 mg/L have been reported (RIVM, 1994). Because the World Health Organization (WHO) drinking-water guideline values for Ni, As, and Sb are 70 μg/L, 10 μg/L, and 20 μg/L, respectively, effective removal methods are needed (WHO, 2011).

Aqueous inorganic As occurs primarily as arsenite, As(III), or arsenate, As(V). Its speciation is influenced by pH and redox potential. As(V) is present in oxidizing environments and exists there as $H_2AsO_4^-$ or $HAsO_4^{2-}$ at pH 4–9. As(III), on the other hand, is present as nonionized H_3AsO_3 when pH is below 7. Moreover, at pH over 7, the proportion of anionic $H_2AsO_3^-$ starts to increase (Smedley and Kinniburgh, 2002). As(III) is more toxic, mobile, and difficult to remove than As(V). Sb, being chemically similar to As, also occurs in aqueous inorganic form as antimonite, Sb(III), and antimonate, Sb(V). The most common species are $Sb(OH)_6^-$ and $Sb(OH)_3$. However, the ecotoxicology, global cycling, and speciation of Sb are not as well-known as those of As (Filella et al., 2002, 2009; Ungureanu et al., 2015). Inorganic Ni is present mainly as bare Ni^{2+} in aqueous solutions at pH 5–9, and complexes with ligands such as OH^-, SO_4^{2-}, HCO_3^-, or Cl^- can also be present (WHO, 2005).

* Corresponding author. Kajaani University of Applied Sciences, Kuntokatu 5, FI-87100, Kajaani, Finland.
E-mail addresses: tero.luukkonen@oulu.fi, teroluuk@gmail.com (T. Luukkonen).

http://dx.doi.org/10.1016/j.jenvman.2015.11.007
0301-4797/

The most commonly used Ni-removal techniques are precipitation, ion flotation, ion exchange, membrane filtration, electrochemical treatment (such as electro-coagulation) and, adsorption (Coman et al., 2013). Due to the chemical resemblance of As and Sb, their removal processes are similar. As- and Sb-removal techniques include, in addition to those mentioned for Ni, conventional coagulation with iron or aluminum chemicals, oxidation, and biological processes (such as phytoremediation, bioremediation, and biofilters) (Ungureanu et al., 2015). Adsorption, due to its ease of operation and simplicity of design, has attracted a great deal of interest as a technique for the removal of Ni, As, and Sb as well as other metals and metalloids from various effluents (Barakat, 2011). Furthermore, the use of various low-cost sorbents such as modified industrial side-products or natural materials is being researched intensively (Iakovleva and Sillanpää, 2013).

The use of geopolymers as sorbents for wastewater treatment is a relatively new area of research. The chemical structure of geopolymers is composed of a negatively charged aluminosilicate framework where charge-balancing cations (such as Na^+, K^+, or Ca^{2+}) can be exchanged with cations in the solution similarly as with zeolites. Metakaolin geopolymers have been studied for the removal of Pb^{2+} (Cheng et al., 2012; López et al., 2014b), Cu^{2+} (Cheng et al., 2012), Cr^{3+} (Cheng et al., 2012), Cd^{2+} (Cheng et al., 2012), Cs^+ (López et al., 2014a, 2014b), and NH_4^+ (Luukkonen et al., 2015). Additionally, coal fly ash geopolymers have been used for the removal of Cu^{2+} (Ge et al., 2015; Mužek et al., 2014; Wang et al., 2007), Pb^{2+} (Al-Zboon et al., 2011), and Cd^{2+} (Javadian et al., 2013). Studies have shown that geopolymerization significantly improves the sorption capacity of the raw material. However, research in this area remains limited. All previous studies have focused on synthetic wastewater, which provides basic knowledge about theoretical removal capacities and kinetics. However, in the treatment of real water matrixes, the presence of competing ions can substantially hinder removal efficiencies.

In this study, batch experiments were used to investigate the capacity of geopolymers prepared with metakaolin (MK) and blast-furnace slag (BFS) to remove Ni(II), As(III) and Sb(III) from a spiked mine effluent. Single-solute and multisolute sorption isotherms together with kinetic models were applied to the data. Geopolymers and their raw materials were characterized according to their physico-chemical properties.

2. Materials and methods

2.1. Materials

The MK sample was obtained from Aquaminerals Finland Ltd. and ground BFS from a Finnish supplier. The sodium silicate (VWR International, SiO_2:Na_2O = 3.1–3.4) and sodium hydroxide (VWR International) used for the synthesis of geopolymers were technical grade.

The mine-effluent sample (settled drainage water treated with ferric sulfate) was obtained from an underground gold mine. The characteristics of the mine-effluent sample as received are shown in Table 1. For comparison, the WHO drinking-water guidelines (WHO, 2011) are shown as a reference. The mine has discharge limits for Ni, As, and Sb: 1000, 500, and 500 μg/L, respectively. $NiCl_2 \cdot 6H_2O$ (Merck), As_2O_3 (Merck) and $SbCl_3$ (Alfa Aesar) were used to prepare the spiked-mine-effluent sample.

2.2. Synthesis of geopolymers

The synthesis of geopolymers was based on the study by Cheng et al. (2012). First, 10 M NaOH solution was mixed with sodium silicate (1:1 w/w) and allowed to stand for 24 h. MK and BFS were mixed with the alkaline solution at ratios (w/w) of 1.3:1 and 3:2, respectively. The formed paste was mixed for 15 min, vibrated for 2 min to remove gas bubbles and, allowed to consolidate at room temperature for 3 days. Geopolymer specimens were crushed and sieved to the particle size of 63–125 μm. Before use, the materials were washed carefully with distilled water, dried at +105 °C, and stored in a desiccator.

Table 1
Characteristics of the mine-effluent sample used in the study. The WHO drinking-water guidelines (WHO, 2011) are presented for reference.

Element	Concentration[a]	WHO drinking-water guideline
SO_4^{2-} [mg/L]	839	–
Cl^- [mg/L]	13	–
NO_3^- [mg/L]	47	50
As [μg/L]	21.8	10
B [μg/L]	65.3	–
Ba [μg/L]	31.4	700
Cd [μg/L]	0.03	3
Co [μg/L]	2.05	–
Cr [μg/L]	1.06	50
Cu [μg/L]	1.02	2000
I [μg/L]	2.39	–
K [mg/L]	18.4	–
Li [μg/L]	3.84	–
Mn [μg/L]	517	–
Mo [μg/L]	19.2	–
Ni [μg/L]	36.5	70
P [μg/L]	23.9	–
Pb [μg/L]	<0.05	–
Rb [μg/L]	48	–
Sb [μg/L]	294	20
Se [μg/L]	1.3	40
Sr [μg/L]	896	–
U [μg/L]	0.42	30
V [μg/L]	0.65	–
Zn [μg/L]	5.92	–
Al [mg/L]	0.2	0.9
Ca [mg/L]	306	–
Fe [mg/L]	<0.05	–
Mg [mg/L]	50.4	–
Na [mg/L]	36.3	–
S [mg/L]	310	–
Si [mg/L]	6.78	–

[a] Determined by an accredited laboratory using an optical emission spectrometer (total concentrations) or an ion chromatograph (anion concentrations).

2.3. Characterization of geopolymers

Powder X-ray diffraction (XRD) patterns were measured with a PanAnalytical Xpert Pro diffractometer. The elemental composition of samples was measured semiquantitatively with an X-ray fluorescence (XRF) spectrometer (PanAnalytical Minipal 4). Fourier transform infrared (FTIR) spectra (650–4000 cm^{-1}) were obtained using a Perkin Elmer Spectrum One spectrometer equipped with an attenuated total reflectance unit. Specific surface area and pore volumes of samples were determined from N_2 gas adsorption–desorption isotherms using a Micrometrics ASAP 2020 instrument. Specific surface area was calculated based on the Brunauer–Emmett–Teller (BET) isotherm, and pore-size distributions were calculated from desorption data using the Barrett–Joyner–Halenda (BJH) method.

2.4. Sorption experiments

The effects of pH, sorbent dose and contact time on the simultaneous removal of Ni, As, and Sb were evaluated using separate batch tests. Experiments were conducted at room temperature (20–23 °C) with the mine-effluent sample spiked with Ni, As and Sb salts. The initial concentrations of Ni(II), As(III), and Sb(III) were

2.17, 2.40, and 1.77 mg/L, respectively. The effect of pH was studied by adjusting the solution pH to 4, 6, 8, or 10 with dilute NaOH or HCl and keeping the sorbent dose (5 g/L) and the mixing time (24 h) constant. The effect of sorbent dose was studied by adjusting the pH to 7–8, adding 0–25 g/L of sorbent to separate subsamples, and shaking for 24 h. The data obtained from the effect of sorbent dose series was used to construct the adsorption isotherms. The effect of contact time was studied by adjusting the pH to 7–8, keeping the sorbent dose constant at 5 g/L, and taking samples at different intervals (1–1440 min). Samples were filtered with a 0.45 μm membrane filter and stored in a refrigerator before analysis. The concentrations of Ni, As, and Sb were determined using an optical emission spectrometer (Thermo Electron IRIS Intrepid II XDL Duo) according to the SFS-EN ISO 11885 standard.

2.5. Isotherms

The equilibrium data were described using single and multi-solute Freundlich and Langmuir isotherm models. The experimental equilibrium sorption capacity (q_e, mg/g) was calculated using Equation (1).

$$q_e = \frac{(c_0 - c_e)V}{m_{ads}} \tag{1}$$

where c_0 and c_e are the initial and equilibrium concentrations (mg/L) of Ni, As, or Sb, respectively. V (L) is the volume of the solution and m_{ads} (g) is the dosed amount of sorbent.

The most commonly used two-parameter isotherm models are the Freundlich (1906) and Langmuir (1918) isotherms which can be expressed with Equations (2) and (3), respectively (Worch, 2012).

$$q_e = Kc_e^n \tag{2}$$

$$q_e = \frac{q_m b c_e}{1 + bc_e} \tag{3}$$

The parameter K is the sorption coefficient [(mg/g)/(mg/L)^n] characterizing the strength of sorption. Higher K indicates higher potential for sorbent loading. The exponent n indicates the energetic heterogeneity of the sorbent surface. Isotherms with $n < 1$ are referred to as favorable and those with $n > 1$ as unfavorable. The parameter q_m is the maximum sorption capacity (mg/g), and b is an empirical constant (L/mg). The Freundlich isotherm model is purely empirical in nature and not well suited for describing very low- or high-concentration areas of the equilibrium data (Worch, 2012). On the other hand, Langmuir isotherm model assumes that only a monolayer sorption occurs, that the surface is energetically homogenic and, that there are no interactions between adsorbed adsorbates.

Multisolute sorption can be described with the extended Langmuir isotherm (Butler and Ockrent, 1930) (Equation (4)) (Worch, 2012).

$$q_{e,i} = \frac{q_{m,\,i} b_i c_i}{1 + \sum_{j=1}^{N} b_j c_j} \tag{4}$$

The parameters q_m and b are the same as in their respective single–solute isotherm equations. It has been shown that the extended Langmuir isotherm is thermodynamically feasible only in cases where all adsorbates have same q_m value (i.e., where $q_{m,1} = q_{m,2} = q_{m,3}$).

Another multisolute isotherm model is the Freundlich isotherm for N components (DiGiano et al., 1978) (Equation (5)), which assumes that all adsorbates have a similar value for the Freundlich exponent, n, and differ only in their sorption coefficient (K) (Worch, 2012).

$$q_i = \frac{K_i^{1/n} c_i}{\left(\sum_{j=1}^{N} K_j^{1/n} c_j\right)^{1-n}} \tag{5}$$

Isotherm parameters were obtained using nonlinear regression with the Microsoft Excel solver tool (GRG nonlinear). The coefficient of determination (R^2), the residual root mean square error (RMSE) and the chi-squared test (χ^2) were used to evaluate model fit and the similarity of the model to the experimental data, respectively (Equations (6)–(8)). Smaller RMSE and χ^2 values indicate better fit and closer similarity between experimental and calculated results. The term p in Equation (7) is the number of parameters employed in the model.

$$R^2 = 1 - \frac{\sum_{n=1}^{n}\left(q_{e,exp,n} - q_{e,model,n}\right)^2}{\sum_{n=1}^{n}\left(q_{e,exp,n} - \overline{q_{e,exp,n}}\right)^2} \tag{6}$$

$$RMSE = \sqrt{\frac{1}{n-p}\sum_{n-1}^{n}\left(q_{e,exp,n} - q_{e,model,n}\right)^2} \tag{7}$$

$$X^2 = \sum_{n=1}^{n}\frac{\left(q_{e,exp,n} - q_{e,model,n}\right)^2}{q_{e,exp,n}} \tag{8}$$

2.6. Kinetics

The kinetic models employed in this study were the pseudo-first-order equation (Lagergren's equation), the pseudo-second-order equation (Ho's equation), Elovich equation, and the Weber–Morris model.

The pseudo-first-order rate equation (Lagergren, 1898) (Equation (9)) is one of the most widely used for describing sorption kinetics from aqueous solutions. The parameter k_1 is the pseudo-first-order rate constant (1/min). Equation (9) can be integrated with the condition $q_t = 0$ when $t = 0$ which results the Equation (10).

$$\frac{dq}{dt} = k_1(q_e - q_t) \tag{9}$$

$$ln\frac{(q_e - q_t)}{q_e} = -k_1 t \tag{10}$$

The pseudo-second-order rate equation (Ho and McKay, 1999) (Equation (11)) can be integrated with $q_t = 0$ when $t = 0$ to obtain Equation (12). The parameter k_2 is the pseudo-second-order rate equilibrium constant [g/(mg min)].

$$\frac{dq_t}{dt} = k_2(q_e - q_t)^2 \tag{11}$$

$$\frac{t}{q_t} = \frac{1}{k_2 q_e^2} + \frac{t}{q_e} \tag{12}$$

The Elovich equation (Zeldowitsch, 1934) (Equation (13)) integration ($q_t = 0$ when $t = 0$) results in Equation (14). The parameter υ_0 [mg/(g min)] is the initial sorption rate, and β (g/mg) is the desorption constant; they can be obtained from the intercept and the slope of q_t vs. ln t plot, respectively.

$$\frac{dq_t}{dt} = v_0 e^{-\beta q_t} \quad (13)$$

$$q_t = \frac{1}{\beta}\ln(v_0\beta) + \frac{1}{\beta}\ln t \quad (14)$$

The Weber–Morris model (Equation (15)) (Weber and Morris, 1963) can be used to evaluate whether the rate-limiting step in the reaction is the boundary-layer (film) or the intraparticle (pore) diffusion of a solute to the surface of the sorbent from the bulk of the solution. The parameter k_{id} [mg/(g min$^{0.5}$)] is the intraparticle diffusion rate constant and C (dimensionless) is the intercept related to the thickness of the boundary layer.

$$q_t = k_{id}t^{0.5} + C \quad (15)$$

2.7. Ni, As, and Sb speciation modeling

MineQL + version 4.6 was used to model As, Ni, and Sb speciation in the pH range 4–12. The input concentration values were 3.34×10^{-5} M for As^{3+} as AsO_3^{3-}, $4.09 \cdot 10^{-5}$ M for Ni^{2+}, and $1.81 \cdot 10^{-5}$ M for Sb^{3+} as $Sb(OH)_3$. MineQL+ is a computational chemical equilibrium modeling system that performs mass balance calculations through a Newton–Raphson method using equilibrium constants from a thermodynamic database.

3. Results and discussion

3.1. Sorbent characterization

Fig. 1 and Table 2 present the crystalline phases and the chemical composition of geopolymers and their raw materials. BFS contains no crystalline phases, and thus a broad amorphous halo at approximately 35° is observed in Fig. 1a. According to Davidovits (2011), the main amorphous phases present in BFS are gehlenite, $Ca_2Al(AlSiO_7)$, and akermanite, $Ca_2Mg(Si_2O_7)$, (Fig. 2) of which gehlenite is the potential geopolymeric precursor. Alkali treatment of BFS results in the formation of hydrotalcite, $Mg_6Al_2CO_3(OH)_{16}\cdot 4(H_2O)$, and hatrurite, Ca_3SiO_5. The formation of hydrotalcite results from the precipitation of free hydroxides—$Al(OH)_3$, $Mg(OH)_2$, and $Ca(OH)_2$—during alkalization and reaction with atmospheric CO_2 (Davidovits, 2011). After the geopolymerization of BFS, the amounts of Al and Si are reduced, whereas Na and loss on ignition (LOI) are increased. Na is incorporated into the geopolymer structure from the alkaline solution and the LOI increase indicates a water content increase. MK contains muscovite, $KAl_2(AlSi_3O_{10})(OH)_2$, and quartz, SiO_2. The metakaolin mineral itself is amorphous and thus produces a broad amorphous halo at approximately 30°. Geopolymerization decreases the muscovite peaks' intensities and causes a small shift of the amorphous halo maximum, indicating a change in the chemical structure. MK contains mainly silicon and aluminum, together with potassium and iron impurities (Table 2). LOI is 3.6% indicating that MK is almost completely calcined, because no further mass loss takes place. After geopolymerization, similarly to BFS, the aluminum and silicon contents are decreased, whereas Na and LOI are increased.

Table 2
Elemental composition and loss on ignition (LOI) at 950 °C of blast-furnace slag (BFS), blast-furnace-slag geopolymer (BFS-GP), metakaolin (MK), and metakaolin geopolymer (MK-GP).

Composition [%]	BFS	BFS-GP	MK	MK-GP
Al_2O_3	8.42	5.87	40.3	31.3
SiO_2	27.20	25.81	53.1	50.7
K_2O	0.55	0.45	2.72	2.19
CaO	38.47	29.87	0.06	0.09
Fe_2O_3	0.78	0.71	1.89	1.6
TiO_2	1.28	1.04	0.12	0.14
MgO	9.39	6.38	–	0.9
SO_3	3.76	2.66	–	–
Mn	0.26	0.21	–	–
Na_2O	0.03	8.00	–	8.16
LOI	0.46	12.92	3.6	8.26

Table 3 presents specific surface areas, average pore widths, and volumes of the geopolymers and their raw materials. The specific surface area increases substantially during the geopolymerization of BFS and MK from 2.79 m^2/g to 64.5 m^2/g and from 11.5 m^2/g to 22.4 m^2/g, respectively. Macro- and mesopore volumes, together with micropore volumes, increase during the geopolymerization of BFS, whereas only macro- and mesopore volumes increase during the geopolymerization of MK. Average pore width decreases during BFS geopolymerization, but it increases during MK geopolymerization. As the specific surface area and pore volumes increase, more sorption sites are available which partly explains the higher sorption capacity of geopolymers when compared to raw materials.

Fig. 3 shows the FTIR spectra of the geopolymers and their raw materials. MK-GP has weak absorbed atmospheric water bands

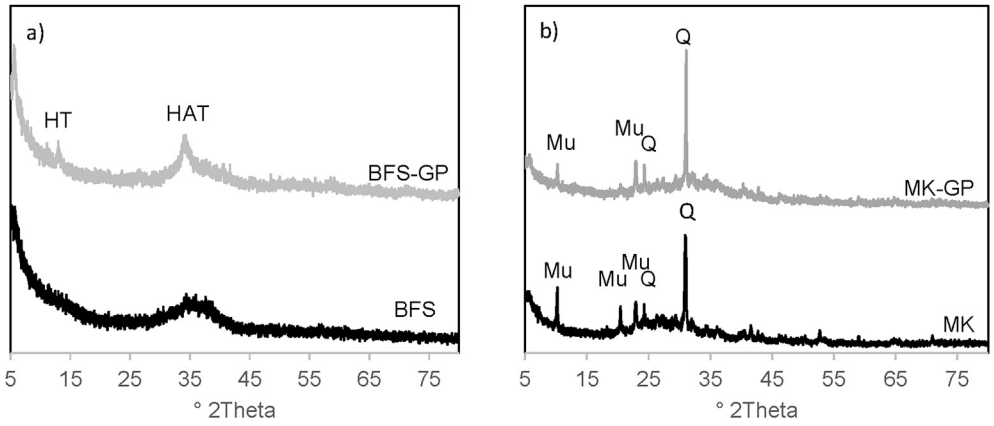

Fig. 1. Diffractograms of a) blast-furnace slag (BFS) and blast-furnace-slag geopolymer (BFS-GP) and b) metakaolin (MK) and metakaolin geopolymer (MK-GP). HT = hydrotalcite, HAT = hatrurite, Mu = muscovite, and Q = quartz.

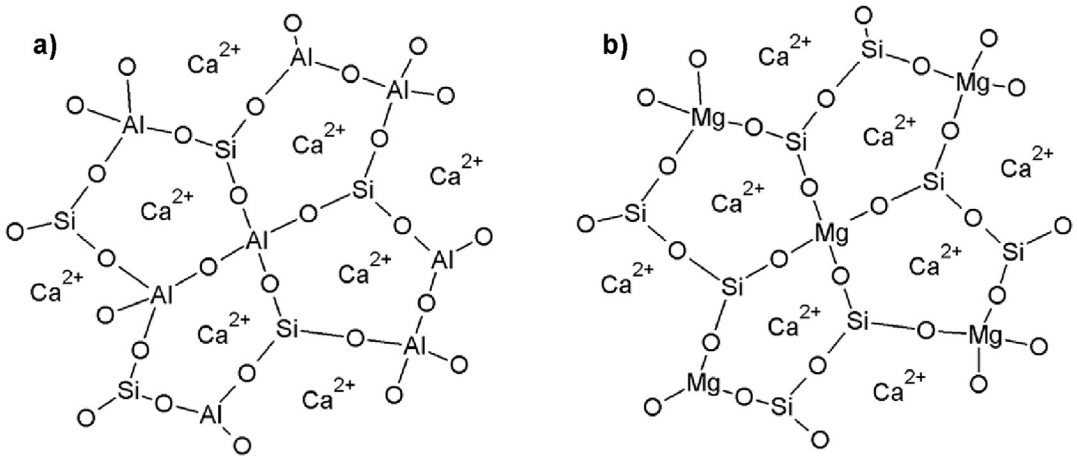

Fig. 2. Conceptual presentation of the most common glassy phases in blast-furnace slag: a) gehlenite and b) akermanite (Davidovits, 2011).

Table 3
Specific surface area, average pore width, and pore volumes of blast-furnace slag (BFS), blast-furnace-slag geopolymer (BFS-GP), metakaolin (MK) and metakaolin geopolymer (MK-GP).

	BFS	BFS-GP	MK	MK-GP
Specific surface area [m^2/g]	2.79	64.5	11.5	22.4
Average pore width [nm]	12.7	5.93	18.17	30.97
Macro- and mesopore volume [cm^3/g][a]	0.008	0.070	0.047	0.165
Micropore volume [cm^3/g][b]	0.001	0.025	0.005	0.008

[a] =macropores: $d_0 > 50$ nm, mesopores: 2 nm $\leq d_0 \leq 50$ nm.
[b] =micropores: $d_0 < 2$ nm.

occurring at 3315 and 1645 cm^{-1} (Barbosa et al., 2000). The strong bands at 970 cm^{-1} and 684 cm^{-1} are the Si–O stretching vibration and the Si–O–Al vibration, respectively, both of which are shifted approximately 90 cm^{-1} during geopolymerization (Barbosa et al., 2000). This indicates a microstructure change or reorganization of the Si environment during geopolymerization (Davidovits, 2011). The strong band present at 894 cm^{-1} in the BFS FTIR spectrum is related to the Si–O stretching. However, during BFS geopolymerization, there is no shift similar to the one that occurs during MK geopolymerization. This indicates that BFS geopolymerization does not involve changes in chemical structure similar to those that take place in the case of MK geopolymerization. The weak band present at approximately 1390 cm^{-1} is probably related to the carbonate vibration (Barbosa et al., 2000). If NaOH is used excessively during geopolymerization the formation of carbonates occurs on the surface of geopolymers as a result of the reaction with atmospheric CO_2 gas.

3.2. Effects of pH, sorbent dose and contact time on the efficiency of Ni, As, and Sb removal

The effect of the initial solution pH is shown in Fig. 4 where the points with the highest removal are highlighted. The sorbent addition increased the solution pH approximately two units during 24 h equilibrating, although materials were carefully washed. Ni removal increases as the initial pH increases. The speciation of Ni as a function of pH is shown in Fig. 5b: Ni is present as the soluble Ni^{2+} until pH 8 is reached when the proportion of the precipitated $Ni(OH)_2$ increases sharply. Consequently, Ni removal with initial pH over 6 (final pH approx. 8) is due partly to the precipitation. However, the results obtained at the initial pH of 4 (final pH approx. 6), when Ni is still soluble, indicate that the sorption-based Ni-

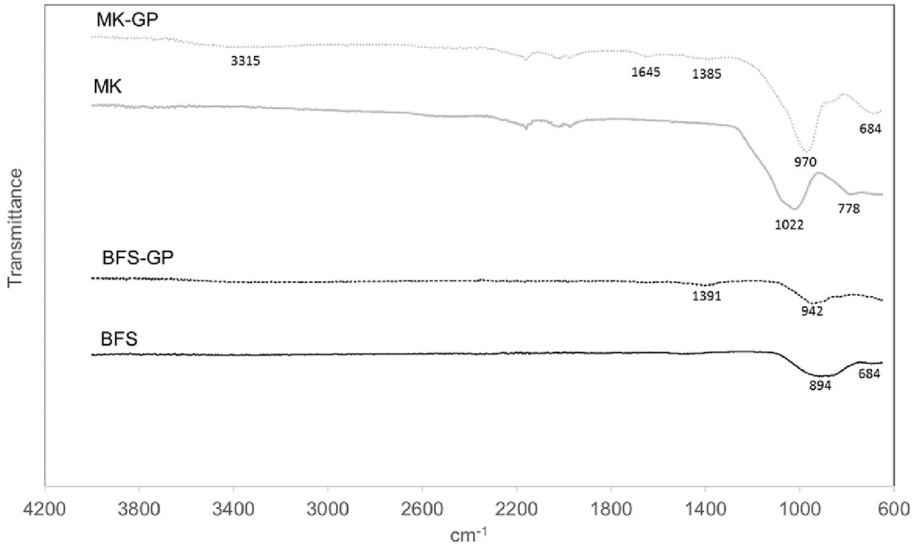

Fig. 3. FTIR spectra of blast-furnace slag (BFS), blast-furnace-slag geopolymer (BFS-GP), metakaolin (MK), and metakaolin geopolymer (MK-GP).

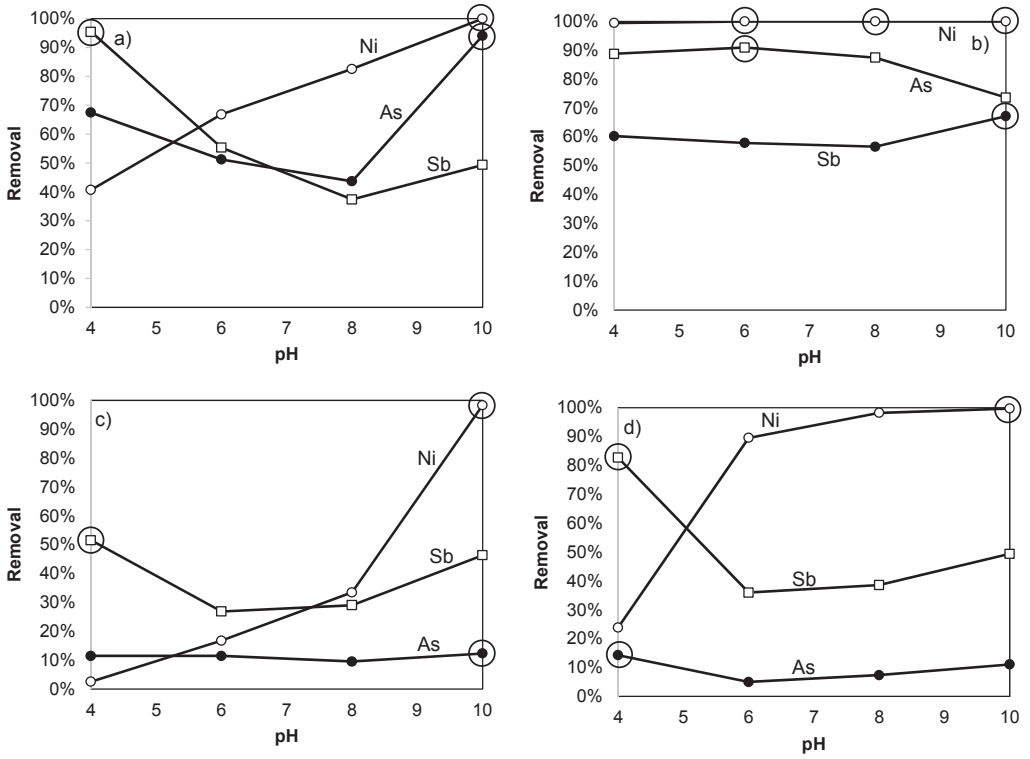

Fig. 4. Effect of initial solution pH on the simultaneous removal of Ni (○), As (●), and Sb (□) with a) blast-furnace slag, b) blast-furnace-slag geopolymer, c) metakaolin, and d) metakaolin geopolymer. The points with the highest removal are highlighted with circles.

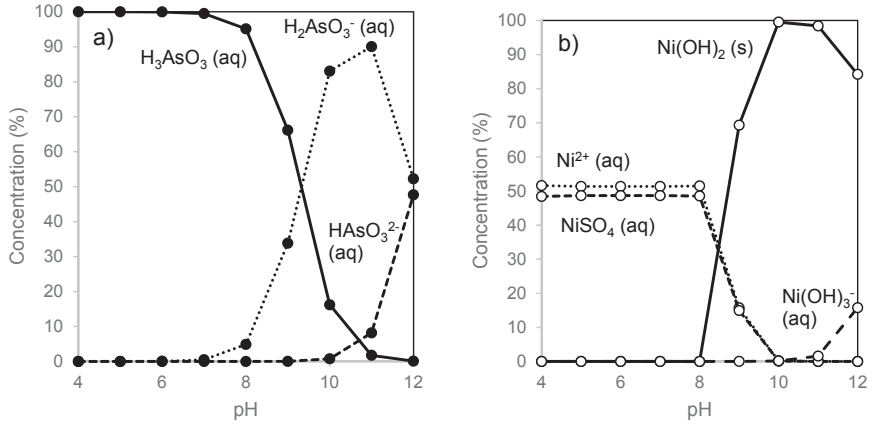

Fig. 5. Speciation of a) As(III) and b) Ni(II) in the water matrix in the pH range 4–12. Sb(III) was present as neutral $Sb(OH)_3$ across the entire pH range.

removal efficiency order is BFS-GP > BFS > MK-GP > MK. As removal is the most efficient at pH 10 with BFS and BFS-GP: 67% and 94%, respectively. On the other hand, MK and MK-GP have low (<15%) As-removal efficiency across the entire pH range. As(III) is present in a protonated form, H_3AsO_3, until pH 7 is reached, when the proportion of the anionic $H_2AsO_3^-$ increases, and the proportion of $HAsO_3^{2-}$ starts to increase at pH over 10. The results indicate that BFS-GP and BFS exhibit a preference for the removal of anionic forms. The hydrotalcite present in BFS-GP has anion-exchange properties that may explain the effective removal of anionic As species (Châtelet et al., 1996; Parker et al., 1995). Sb removal is more efficient at lower pH area and it decreases sharply as pH is increased. However, BFS-GP exhibits over 88% removal until pH 8 is reached, when the removal efficiency starts to decrease. Sb is present as the electrically neutral $Sb(OH)_3$ in the pH range of 4–12 (not shown in Fig. 5).

The effect of sorbent dose is shown in Fig. 6. The sorbent dose after which the removal percentage starts to level off represent the optimum from the techno-economical point of view (highlighted in Fig. 6). The selectivity for BFS, MK, and MK-GP is Ni(II) > As(III) > Sb(III), whereas for BFS-GP the selectivity is Ni(II) > As(III) ≈ Sb(III). In the case of BFS, geopolymerization clearly increases the efficiency of Ni, As, and Sb removal (Fig. 6a and b). However, the geopolymerization of MK only slightly enhances the removal of Ni, reduces the removal of As, and leaves Sb unaltered (Fig. 6c and d). The reduced As removal in the case of MK

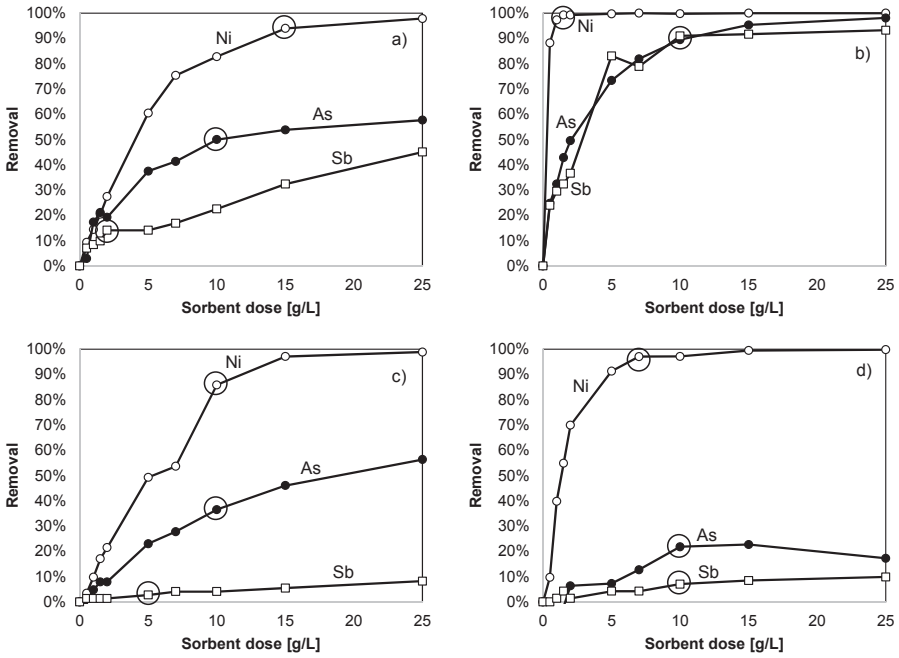

Fig. 6. Effect of sorbent dose on the simultaneous removal of Ni (○), As (●), and Sb (□): a) blast-furnace slag, b) blast-furnace-slag geopolymer, c) metakaolin, and d) metakaolin geopolymer. The removal percentage starts to level off after highlighted points.

compared to that in the case MK-GP may result from the presence of anionic forms of As ($H_2AsO_3^-$ and $HAsO_3^{2-}$): MK-GP is essentially a cation exchanger and thus repulses anions (Luukkonen et al., 2015).

The effect of contact time is shown in Fig. 7. BFS-GP involves a clear improvement over BFS with respect to the kinetics of Ni, As and Sb removal as shown in Fig. 7a and b, respectively. However, MK-GP involves an improvement over MK only with respect to the removal kinetics of Ni; geopolymerization leaves As and Sb removal unaltered (Fig. 7c and d). BFS-GP reaches equilibrium for Ni, As, and Sb removal after approximately 6 h contact time. On the other hand, the data for MK and MK-GP suggest that Ni removal equilibrium is not completely achieved after 24 h contact time, whereas As and Sb removal (which is <10%) reaches equilibrium after only

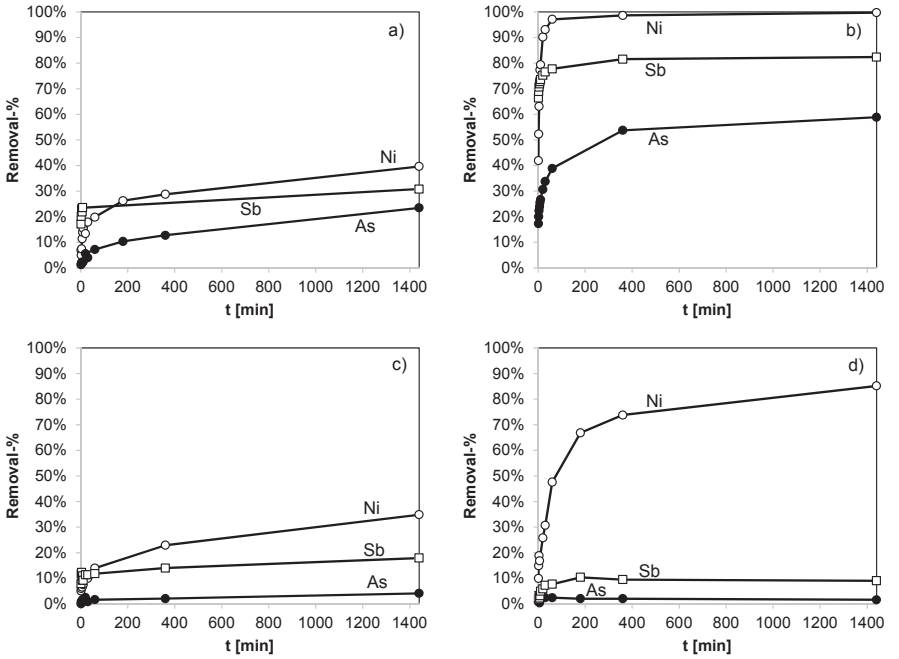

Fig. 7. Effect of contact time on the simultaneous removal of Ni (○), As (●), and Sb (□): a) blast-furnace slag, b) blast-furnace-slag geopolymer, c) metakaolin, and d) metakaolin geopolymer.

Table 4
Parameters of the kinetic models.

		MK			MK-GP			BFS			BFS-GP		
		As	Ni	Sb	As	Ni	Sb	As	Ni	Sb	As	Ni	Sb
	q_e [mg/g]	0.014	0.269	0.068	0.008	0.335	0.066	0.115	0.156	0.140	0.293	0.395	0.382
Pseudo-first-order	k_1 [1/min]	0.005	0.002	0.007	0.058	0.005	0.030	0.002	0.003	0.066	0.006	0.010	0.008
	R^2	0.673	0.971	0.693	0.175	0.877	0.887	0.910	0.834	0.767	0.963	0.634	0.909
Pseudo-second-order	q_{calc} [mg/g]	0.014	0.28	0.069	0.008	0.338	0.067	0.118	0.157	0.141	0.294	0.395	0.382
	k_2 [g/(mg min)]	3.137	0.025	1.996	−13.911	0.119	10.944	0.080	0.168	3.866	0.233	1.124	1.702
	R^2	0.987	0.912	0.999	0.997	0.998	0.9998	0.954	0.990	1	0.999	1	1
Elovich equation	β [g/mg]	476.19	33.11	256.4	1250	23.364	178.57	72.993	34.843	128.21	32.573	31.447	95.238
	υ_0 [mg/(g min]	0.003	0.011	88.13	0.683	0.090	2.606	0.006	0.013	566.05	0.300	31.140	1.1E11
	R^2	0.669	0.755	0.675	0.292	0.941	0.848	0.858	0.953	0.916	0.978	0.783	0.966

MK = metakaolin, MK-GP = metakaolin geopolymer, BFS = blast-furnace slag and BFS-GP = blast-furnace-slag geopolymer.

180 min.

3.3. Isotherms

Isotherms provide information about the distribution of adsorbate between liquid and solid (sorbent) phases at the equilibrium state. Sorption can be described with single–solute isotherms, of which the most commonly used are the Langmuir and Freundlich models. However, in real wastewaters, there are usually several adsorbates competing for the same sorption sites. As a general trend, the higher valence and atomic number results a higher affinity for a sorption site. In the present case, the most important competing ions with Ni(II), As(III), and Sb(III) are cations Sr^{2+}, Mn^{2+}, Ca^{2+}, and Mg^{2+}, whereas the anions that are present (SO_4^{2-}, NO_3^-, and Cl^-) are not easily adsorbed (see Table 1 for concentrations). Simultaneous sorption can be described with the multisolute isotherms. Typically, the extent of sorption decreases in the presence of competing adsorbates compared to simple single adsorbate sorption (Oh and Kim, 2014).

Generally, the fitting of experimental sorption data with the isotherm models was frequently poor which could be due to the fact that equilibrium was not completely achieved as suggested by results shown in Fig. 7. The isotherm parameters and graphs are shown in supplementary material. BFS-GP proved to be the most prominent material for Ni(II), As(III), and Sb(III) removal and therefore only its fitting to isotherms is discussed. Ni-removal with BFS-GP is best described with the Langmuir isotherm ($R^2 = 0.968$). The maximum Ni-removal capacity is 4.418 mg/g, which is significantly higher than the maximum Ni-removal capacity of the raw material BFS: 0.332 mg/g. This clearly demonstrates the positive effect of geopolymerization. As(III) and Sb(III) removal with BFS-GP exhibits a best fit with the multisolute Freundlich isotherm (R^2 = 0.949 and 0.772). However, the multisolute Freundlich parameter n is > 1 in both cases, indicating an unfavorable sorption process.

3.4. Kinetics

The parameters of kinetic models obtained by linear regression are shown in Table 4. The best fits (R^2 values) were obtained with the pseudo-second-order kinetic model, with the exception of Ni removal with MK, for which the best model was the pseudo-first-order kinetic model. Graphs of t vs. t/q_t (pseudo-second-order model) and t vs. $ln[(q_e\text{-}q_t)/q_e]$ (pseudo-first-order model) are shown in supplementary materials. Pseudo-second-order rate constants (k_2) indicate the following order for Ni removal: BFS-GP > BFS > MK-GP > MK; for As removal: MK > BFS-GP > BFS > MK-GP; and for Sb removal: MK-GP > BFS > MK > BFS-GP. Experimental capacity values (q_e) are in good agreement with calculated capacities (q_{calc}).

The Weber-Morris plot (graph shown in supplementary materials) indicates that the sorption process consists of several phases. Furthermore, because the plots are not passing through origin, the rate-limiting step is not the pore (i.e. intraparticle) diffusion but the film (i.e., boundary-layer) diffusion. The first phases of sorption are related to the attachment to the most readily available surface sites, whereas the latter phases involve the slow diffusion of adsorbate from the surface to the inner pores (Runtti et al., 2014).

3.5. Comparison to other sorbents

Table 5 presents examples of results reported in the literature. In this study, the best Ni-removal results were obtained with BFS-GP ($q_m = 4.4$ mg/g). Dimitrova and Mehanjiev (2000) and Gupta (1998) reported 55.76 mg/g and 30 mg/g Ni-removal capacity for BFS and thermally activated BFS, respectively. However, the water matrix in these studies was synthetic wastewater, which resulted in theoretical maximum capacity values. In our study, competing ions were present, which decreased the obtained capacity. As(III) removal from synthetic wastewaters has resulted in maximum capacities of 0.82 and 30.1 with BFS and Fe_2O_3-loaded melted slag (Lekic et al., 2013; Zhang and Itoh, 2005). As(III) removal with BFS-GP ($q_{exp} = 0.52$ mg/g) was comparatively low in the present study, but again the water matrix decreased the capacity. As(V) is typically sorbed more readily than As(III) (Ungureanu et al., 2015). The Sb(III)-removal capacity of BFS-GP ($q_{exp} = 0.34$ mg/g) was clearly lower than indicated by the results shown in Table 5. However, Wang et al. (2015) observed that the presence of Ni^{2+} inhibited Sb(V) sorption on Fe-modified aerobic granules, which may have been also the case in the present study. Additionally, in the present study the relatively low initial concentrations of Ni(II), As(III), and Sb(III) (approx. 2 mg/L) cause lower adsorption amounts.

4. Conclusions

Geopolymerization with an alkaline solution (10 M NaOH: sodium silicate = 1:1 w/w) resulted an increase in the surface area and pore volumes of blast-furnace slag and metakaolin. Furthermore, changes in the chemical composition and structure were observed with XRF, XRD, and FTIR measurements. The obtained geopolymers and their raw materials were tested for the treatment of a real mine effluent spiked with Ni(II), As(III), and Sb(III). Blast-furnace-slag geopolymer proved to be more effective sorbent than blast-furnace slag, metakaolin, or metakaolin geopolymer. Geopolymerization of blast-furnace slag increased the capacity of Ni(II), As(III), and Sb(III) removal from 0.33 mg/g, 0.18 mg/g and 0.06 mg/g to 4.42 mg/g, 0.52 mg/g, and 0.34 mg/g, respectively. The relatively low removal capacities are possibly a result of a low initial concentrations of Ni(II), As(III), and Sb(III), competition between adsorbates, and other inhibitive effects related to the water matrix

Table 5
Examples of sorption results for Ni, As and Sb reported in the literature.

Ni							
Sorbent	Capacity [mg/g]	Water matrix	pH	Ni [mg/L]	Sorbent dose [g/L]	T [°C]	Ref.
Kaolinite	0.90[a]	Synthetic (single-adsorbate)	7	10–150	25	30	Jiang et al., 2010
Kaolinite	0.55[a]	Synthetic (multiadsorbate)	7	10–150	25	30	Jiang et al., 2010
Kaolinite	0.02[b]	Copper plating wastewater	8.9	0.74	25	30	Jiang et al., 2010
Kaolinite	0.72[b]	Zincification wastewater	1.9	30	25	30	Jiang et al., 2010
BFS	55.76[b]	Synthetic	4.1	5.9–59	1	25	Dimitrova and Mehanjiev, 2000
Thermally activated BFS	30[a]	Synthetic	4.0	100–250	10	30	Gupta, 1998
PPD modified kaolinite[e]	621.0[a]	Synthetic	5.7	20–8000	8	30	Mekewi et al., 2013
Acid-activated kaolinite	9.9[a]	Synthetic	5.7	10–50	2	30	Bhattacharyya and Gupta, 2008
As							
Sorbent	Capacity [mg/g]	Water matrix	pH	As [mg/L]	Sorbent dose [g/L]	T [°C]	Ref.
Kaolinite	As(III), As(V): <0.23[a]	Synthetic	5.5	10–1000	100	25	Ladeira and Ciminelli, 2004
Kaolinite	As(V): 0.86[a]	Synthetic	5.0	10–200	40	25	Mohapatra et al., 2007
HDTMA-Br modified kaolinite[d]	As(V): 0.97[a]	Synthetic	13	0–247	250	25	Li and Bowman, 2001
HDTMA-Br modified kaolinite[d]	As(III): 0.32[a] As(V): 0.67[a]	Synthetic	6.5–6.8	7–150	100	22	Li et al., 2007
BFS	As(V): 1.27[a]	Synthetic	6.7	1–320	10	25	Hua et al., 2015
BFS	As(III): 0.82[a] As(V): 4.04[a]	Synthetic	7	0.5–100	10	Room temp.	Lekic et al., 2013
Fe_2O_3 loaded melted slag	As(III): 30.1[b] As(V): 78.5[b]	Synthetic	2.5	20–300	4	20	Zhang and Itoh, 2005
Sb							
Sorbent	Capacity [mg/g]	Water matrix	pH	Sb [mg/L]	Sorbent dose [g/L]	T [°C]	Ref.
GO–SCH[f]	Sb(V): 158.6[b]	Synthetic	7.0	0–60	0.3	25	Dong et al., 2015
Fe-modified aerobic granules	Sb(V): 125[a]	Synthetic	3.4	20[c]	2–30	35	Wang et al., 2015
Fe^{2+} -doped Mg–Al double hydroxides	Sb(V): approx. 219[b]	Synthetic	≈3.5–7.5	36.5–73.1	4	30	Kameda et al., 2015
Ferric hydroxide	Sb(III): 101	Synthetic	3.0	24–244	0.2	25	Xu et al., 2011
Manganese dioxide	Sb(III): 98.7	Synthetic	3.0	24–244	0.2	20	Xu et al., 2011
Fe–Mn binary oxide	Sb(III): 214	Synthetic	3.0	24–244	0.2	20	Xu et al., 2011
Goethite	Sb(V): 18.3	Synthetic	7.0	0.05–15	1	25	Xi et al., 2013
Diatomite	Sb(III): 35.2	Synthetic	6	10–400	4	20	Sari et al., 2010
Synthetic manganite	Sb(V): 95	Synthetic	3.0	0.5–98	4	25	Wang et al., 2012

[a] Langmuir maximum sorption capacity, q_m.
[b] Experimental maximum sorption capacity.
[c] Conditions for isotherm data determination not given.
[d] HDTMA-Br = hexadecyltrimethylammonium bromide.
[e] PPD = Polyoxypropylenediamine.
[f] GO-SCH = graphene oxide/schwertmannite nanocomposites.

(real mine effluent). The results indicate that blast-furnace-slag geopolymer could serve as a feasible metal and metalloid sorbent with a specific utilization prospect in the mining industry.

Acknowledgments

This study was conducted as a part of the GeoMaterials (Fimos 118048) and SULKA (A32164, 524/2012) projects which were funded mainly by the Regional Council of Kainuu and the European Union (European Regional Development Fund), respectively. The authors wish to thank Mr. Kai Tiihonen, Ms. Marjukka Hyyryläinen and Ms. Sara Lopéz, all of whom provided valuable help during the study.

Appendix A. Supplementary data

Supplementary data related to this article can be found at http://dx.doi.org/10.1016/j.jenvman.2015.11.007.

References

Al-Zboon, K., Al-Harahsheh, M.S., Hani, F.B., 2011. Fly ash-based geopolymer for Pb removal from aqueous solution. J. Hazard. Mater. 188, 414–421. http://dx.doi.org/10.1016/j.jhazmat.2011.01.133.
An, Y., Kim, M., 2009. Effect of antimony on the microbial growth and the activities of soil enzymes. Chemosphere 74, 654–659. http://dx.doi.org/10.1016/j.chemosphere.2008.10.023.
Barakat, M.A., 2011. New trends in removing heavy metals from industrial wastewater. Arab. J. Chem. 4, 361–377. http://dx.doi.org/10.1016/j.arabjc.2010.07.019.
Barbosa, V.F.F., MacKenzie, K.J.D., Thaumaturgo, C., 2000. Synthesis and characterisation of materials based on inorganic polymers of alumina and silica: sodium polysialate polymers. Int. J. Inorg. Mater. 2, 309–317. http://dx.doi.org/10.1016/S1466-6049(00)00041-6.
Bhattacharyya, K.G., Gupta, S.S., 2008. Influence of acid activation on adsorption of Ni(II) and Cu(II) on kaolinite and montmorillonite: kinetic and thermodynamic study. Chem. Eng. J. 136, 1–13. http://dx.doi.org/10.1016/j.cej.2007.03.005.
Butler, J.A.V., Ockrent, C., 1930. Studies in electrocapillarity. Part III. The surface tensions of solutions containing two surface-active solutes. J. Phys. Chem. 34, 2841–2859.
Châtelet, L., Bottero, J.Y., Yvon, J., Bouchelaghem, A., 1996. Competition between monovalent and divalent anions for calcined and uncalcined hydrotalcite: anion exchange and adsorption sites. Colloids Surf. Physicochem. Eng. Asp. 111,

167–175. http://dx.doi.org/10.1016/0927-7757(96)03542-X.
Cheng, T.W., Lee, M.L., Ko, M.S., Ueng, T.H., Yang, S.F., 2012. The heavy metal adsorption characteristics on metakaolin-based geopolymer. Appl. Clay Sci. 56, 90–96. http://dx.doi.org/10.1016/j.clay.2011.11.027.
Coman, V., Robotin, B., Ilea, P., 2013. Nickel recovery/removal from industrial wastes: a review. Resour. Conserv. Recycl. 73, 229–238. http://dx.doi.org/10.1016/j.resconrec.2013.01.019.
Davidovits, J., 2011. Geopolymer Chemistry & Applications, third ed. Institut Geopolymere, Saint-Quentin, France.
DiGiano, F.A., Baldauf, G., Frick, B., Sontheimer, H.A., 1978. A simplified competitive equilibrium adsorption model. Chem. Eng. Sci. 33, 1667–1673. http://dx.doi.org/10.1016/0009-2509(78)85143-4.
Dimitrova, S.V., Mehanjiev, D.R., 2000. Interaction of blast-furnace slag with heavy metal ions in water solutions. Water Res. 34, 1957–1961. http://dx.doi.org/10.1016/S0043-1354(99)00328-0.
Dong, S., Dou, X., Mohan, D., Pittman, C.U., Luo, J., 2015. Synthesis of graphene oxide/schwertmannite nanocomposites and their application in Sb(V) adsorption from water. Chem. Eng. J. 270, 205–214. http://dx.doi.org/10.1016/j.cej.2015.01.071.
Filella, M., Belzile, N., Chen, Y., 2002. Antimony in the environment: a review focused on natural waters: I. Occurrence. Earth Sci. Rev. 57, 125–176. http://dx.doi.org/10.1016/S0012-8252(01)00070-8.
Filella, M., Williams, P.A., Belzile, N., 2009. Antimony in the environment: knowns and unknowns. Environ. Chem. 6, 95–105. http://dx.doi.org/10.1071/EN09007.
Freundlich, H., 1906. Über die adsorption in lösungen [on the adsorption in solutions]. Z. Phys. Chem. 57, 385–470.
Ge, Y., Cui, X., Kong, Y., Li, Z., He, Y., Zhou, Q., 2015. Porous geopolymeric spheres for removal of Cu(II) from aqueous solution: synthesis and evaluation. J. Hazard. Mater 283, 244–251. http://dx.doi.org/10.1016/j.jhazmat.2014.09.038.
Gupta, V.K., 1998. Equilibrium uptake, sorption dynamics, process development, and column operations for the removal of copper and nickel from aqueous solution and wastewater using activated slag, a low-cost adsorbent. Ind. Eng. Chem. Res. 37, 192–202. http://dx.doi.org/10.1021/ie9703898.
Ho, Y.S., McKay, G., 1999. Pseudo-second order model for sorption processes. Process Biochem. 34, 451–465. http://dx.doi.org/10.1016/S0032-9592(98)00112-5.
Hua, T., Haynes, R.J., Zhou, Y.-., Boullemant, A., Chandrawana, I., 2015. Potential for use of industrial waste materials as filter media for removal of Al, Mo, As, V and Ga from alkaline drainage in constructed wetlands – adsorption studies. Water Res. 71, 32–41. http://dx.doi.org/10.1016/j.watres.2014.12.036.
Iakovleva, E., Sillanpää, M., 2013. The use of low-cost adsorbents for wastewater purification in mining industries. Environ. Sci. Pollut. Res. 20, 7878–7899. http://dx.doi.org/10.1007/s11356-013-1546-8.
IARC, 2012. IARC Monographs on the Evaluation of Carcinogenic Risks to Humans. Arsenic, Metals, Fibres and Dusts, 100C. IARC, Lyon, France.
IARC, 2004. IARC Monographs on the Evaluation of Carcinogenic Risks to Humans. Some Drinking-water Disinfectants and Contaminants, Including Arsenic, 84. IARC, Lyon, France.
IARC, 1990. IARC Monographs on the Evaluation of Carcinogenic Risks to Humans. Chromium, Nickel and Welding, 49. IARC, Lyon, France.
IARC, 1989. IARC Monographs on the Evaluation of Carcinogenic Risks to Humans. Some Organic Solvents, Resin Monomers and Related Compounds, Pigments and Occupational Exposures in Paint Manufacture and Painting, 47. IARC, Lyon, France.
Javadian, H., Ghorbani, F., Tayebi, H., Asl, S.H., 2013. Study of the adsorption of Cd (II) from aqueous solution using zeolite-based geopolymer, synthesized from coal fly ash; kinetic, isotherm and thermodynamic studies. Arab. J. Chem. 8, 837–849. http://dx.doi.org/10.1016/j.arabjc.2013.02.018.
Jiang, M., Jin, X., Lu, X., Chen, Z., 2010. Adsorption of Pb(II), Cd(II), Ni(II) and Cu(II) onto natural kaolinite clay. Desalination 252, 33–39. http://dx.doi.org/10.1016/j.desal.2009.11.005.
Kameda, T., Kondo, E., Yoshioka, T., 2015. Equilibrium and kinetics studies on As(V) and Sb(V) removal by Fe^{2+}-doped Mg-Al layered double hydroxides. J. Environ. Manage. 151, 303–309. http://dx.doi.org/10.1016/j.jenvman.2014.12.050.
Ladeira, A.C.Q., Ciminelli, V.S.T., 2004. Adsorption and desorption of arsenic on an oxisol and its constituents. Water Res. 38, 2087–2094. http://dx.doi.org/10.1016/j.watres.2004.02.002.
Lagergren, S., 1898. Zur theorie der sogenannten adsorption gelöster stoffe [About the theory of so-called adsorption of soluble substances. K. Sven. Vetenskapsakademiens 1–39. Handlingar Band 24, No. 4.
Langmuir, I., 1918. The adsorption of gases on plane surfaces of glass, mica and platinum. J. Am. Chem. Soc. 40, 1361–1403.
Lehr, C.R., Kashyap, D.R., McDermott, T.R., 2007. New insights into microbial oxidation of antimony and arsenic. Appl. Environ. Microbiol. 73, 2386–2389. http://dx.doi.org/10.1128/AEM.02789-06.
Lekic, B.M., Markovic, D.D., Rajakovic-Ognjanovic, V.N., Dukic, A.R., Rajakovic, L.V., 2013. Arsenic removal from water using industrial By-products. J. Chem. 2013. http://dx.doi.org/10.1155/2013/121024.
Li, Z., Beachner, R., McManama, Z., Hanlie, H., 2007. Sorption of arsenic by surfactant-modified zeolite and kaolinite. Microporous Mesoporous Mater. 105, 291–297. http://dx.doi.org/10.1016/j.micromeso.2007.03.038.
Li, Z., Bowman, R.S., 2001. Retention of inorganic oxyanions by organo-kaolinite. Water Res. 35, 3771–3776. http://dx.doi.org/10.1016/S0043-1354(01)00120-8.
López, F.J., Sugita, S., Kobayashi, T., 2014a. Cesium-adsorbent geopolymer foams based on silica from rice husk and metakaolin. Chem. Lett. 43, 128–130. http://doi.org/10.1246/cl.130851.
López, F.J., Sugita, S., Tagaya, M., Kobayashi, T., 2014b. Metakaolin-based geopolymers for targeted adsorbents to heavy metal ion separation. J. Mater. Sci. Chem. Eng. 2, 16–27. http://dx.doi.org/10.4236/msce.2014.27002.
Luukkonen, T., Sarkkinen, M., Kemppainen, K., Rämö, J., Lassi, U., 2015. Metakaolin geopolymer characterization and application for ammonium removal from model solutions and landfill leachate. Appl. Clay Sci. (in press), accepted manuscript http://dx.doi.org/10.1016/j.clay.2015.10.027.
Mekewi, M.A., Darwish, A.S., Amin, M.E., Bourazan, H.A., 2013. Sustainable removal of Cu^{2+}, Ni^{2+} and Zn^{2+} ions from severe contaminated water using kaolin/poly(glycine) composites, characterization and uptake studies. Desalin. Water Treat. 51, 7746–7763. http://dx.doi.org/10.1080/19443994.2013.792491.
Mohapatra, D., Mishra, D., Chaudhury, G.R., Das, R.P., 2007. Arsenic(V) adsorption mechanism using kaolinite, montmorillonite and illite from aqueous medium. J. Environ. Sci. Health A Tox. Hazard Subst. Environ. Eng. 42, 463–469. http://dx.doi.org/10.1080/10934520601187666.
Mužek, M.N., Svilovic, S., Zelic, J., 2014. Fly ash-based geopolymeric adsorbent for copper ion removal from wastewater. Desalin. Water Treat. 52, 2519–2526. http://dx.doi.org/10.1080/19443994.2013.792015.
Oh, S., Kim, D.S., 2014. Adsorption features of heavy metal ions on activated carbon in single and multisolute systems. J. Environ. Sci. Health A Tox. Hazard Subst. Environ. Eng. 49, 710–719. http://dx.doi.org/10.1080/10934529.2014.865460.
Parker, L.M., Milestone, N.B., Newman, R.H., 1995. The use of hydrotalcite as an anion absorbent. Ind. Eng. Chem. Res. 34, 1196–1202. http://dx.doi.org/10.1021/ie00043a023.
RIVM, 1994. Attention Substances in Dutch Environmental Policy (Report No. 601014). Rijkinstitut voor Volksgezondheid en Milieuhygiene (National Institute of Public Health and Environmental Protection), Bilthoven, Netherlands.
Runtti, H., Tuomikoski, S., Kangas, T., Lassi, U., Kuokkanen, T., Rämö, J., 2014. Chemically activated carbon residue from biomass gasification as a sorbent for iron (II), copper (II) and nickel (II) ions, J. Water Process Eng. 4, 12–24. http://dx.doi.org/10.1016/j.jwpe.2014.08.009.
Sari, A., Çitak, D., Tuzen, M., 2010. Equilibrium, thermodynamic and kinetic studies on adsorption of Sb(III) from aqueous solution using low-cost natural diatomite. Chem. Eng. J. 162, 521–527. http://dx.doi.org/10.1016/j.cej.2010.05.054.
Serfor-Armah, Y., Nyarko, B.J.B., Adotey, D.K., Dampare, S.B., Adomako, D., 2006. Levels of arsenic and antimony in water and sediment from Prestea, a gold mining town in Ghana and its environs. Water Air Soil Pollut. 175, 181–192. http://dx.doi.org/10.1007/s11270-006-9127-9.
Smedley, P., Kinniburgh, D., 2002. A review of the source, behaviour and distribution of arsenic in natural waters. Appl. Geochem 17, 517–568. http://dx.doi.org/10.1016/S0883-2927(02)00018-5.
Ungureanu, G., Santos, S., Boaventura, R., Botelho, C., 2015. Arsenic and antimony in water and wastewater: overview of removal techniques with special reference to latest advances in adsorption. J. Environ. Manage. 151, 326–342. http://dx.doi.org/10.1016/j.jenvman.2014.12.051.
Wang, L., Wan, C., Zhang, Y., Lee, D., Liu, X., Chen, X., Tay, J., 2015. Mechanism of enhanced Sb(V) removal from aqueous solution using chemically modified aerobic granules. J. Hazard. Mater 284, 43–49. http://dx.doi.org/10.1016/j.jhazmat.2014.10.041.
Wang, S., Li, L., Zhu, Z.H., 2007. Solid-state conversion of fly ash to effective adsorbents for Cu removal from wastewater. J. Hazard. Mater 139, 254–259. http://dx.doi.org/10.1016/j.jhazmat.2006.06.018.
Wang, X., He, M., Lin, C., Gao, Y., Zheng, L., 2012. Antimony(III) oxidation and antimony(V) adsorption reactions on synthetic manganite. Chem. Erde Geochem 72, 41–47. http://dx.doi.org/10.1016/j.chemer.2012.02.002.
Weber, W.J., Morris, J.C., 1963. Kinetics of adsorption on carbon from solution. J. Sanit. Eng. Div. Am. Soc. Civ. Eng. 89, 31–60.
WHO, 2011. Guidelines for Drinking-water Quality, fourth ed. World Health Organization, Geneva, Switzerland.
WHO, 2005. Nickel in Drinking-water. Background Document for Development of WHO Guidelines for Drinking-water Quality (WHO/SDE/WSH/05.08/55). World Health Organization, Geneva, Switzerland.
Worch, E., 2012. Adsorption Technology in Water Treatment: Fundamentals, Processes, and Modelling. Walter de Gruyter, Berlin, Germany.
Xi, J., He, M., Wang, K., Zhang, G., 2013. Adsorption of antimony(III) on goethite in the presence of competitive anions. J. Geochem. Explor 132, 201–208. http://dx.doi.org/10.1016/j.gexplo.2013.07.004.
Xu, W., Wang, H., Liu, R., Zhao, X., Qu, J., 2011. The mechanism of antimony(III) removal and its reactions on the surfaces of Fe-Mn binary oxide. J. Colloid Interface Sci. 363, 320–326. http://dx.doi.org/10.1016/j.jcis.2011.07.026.
Zeldowitsch, J., 1934. Über den mechanismus der katalytischen oxydation von CO an MnO_2 [About the mechanism of catalytic oxidation of CO over MnO_2]. Acta Physicochim. URSS 1, 364–449.
Zhang, F., Itoh, H., 2005. Iron oxide-loaded slag for arsenic removal from aqueous system. Chemosphere 60, 319–325. http://dx.doi.org/10.1016/j.chemosphere.2004.12.019.